FIZIKA 9 (1977) Supplement 4, 559–594
(Proceedings of the Int. Symp. on Nuclear Collisions and
Their Microscopic Description, Bled, September 1977)

FRAGMENTATION IN FISSION, FUSION AND HEAVY ION SCATTERING*

K.H. Ziegenhain, H.J. Lustig, J. Hahn, J.A. Maruhn and W. Greiner
Institut für Theoretische Physik der Johann Wolfgang Goethe-Universität,
Frankfurt
and
W. Scheid**
Institut für Theoretische Physik der Justus-Liebig-Universität, Giessen

1. Introduction

In this paper we discuss a consistent method to treat two-body breakup channels in fission, fusion and heavy ion scattering. Two-body breakup channels can be described in the framework of the fragmentation theory which is the main subject of this article. Review articles about the theory of fragmentation are listed as Refs. 1-3.

The basic idea of the theory of fragmentation is the introduction of the collective mass fragmentation coordinate[4] which is defined by $\eta = (A_1-A_2)/(A_1+A_2)$ for separated nuclei with nucleon numbers A_1 and A_2. This coordinate has the range $-1 \leq \eta \leq 1$ and describes the symmetric fragmentation, i.e. two equal nuclei, for $\eta = 0$ and the completely fused system for $\eta = \pm 1$. Whereas one is already accustomed to treat heavy-ion collisions with the relative coordinate between the nuclei and coordinates for nuclear surface excitations, we suggest the idea to treat the fragmentation coordinate in exactly the same manner as other dynamic collective coordinates on which the wave functions depend. Therefore, the fragmentation degree of freedom allows us to describe the few-nucleon, multinucleon and cluster transfer, the complete and incomplete fusion and the fission of the compound nucleus in an unifying method. Beside the mass fragmentation coordinate also a charge fragmentation coordinate has been suggested[5] which is analogously defined as $\eta_Z=(Z_1-Z_2)/(Z_1+Z_2)$ where Z_1 and Z_2 are the charge numbers of the fragments.

Let us consider the advantages of introducing the mass fragmentation as a coordinate[6]. After quantizing the fragmentation degree of freedom the wave

* Work supported by the Bundesministerium für Forschung und Technologie (BMFT) and by the Gesellschaft für Schwerionenforschung (GSI)

** Talk presented by W. Scheid

function depends on the η-coordinate: $\psi(\vec{R},\eta,t)$. The square of the absolute value of the wave function is proportional to the probability $w(\eta)$ for finding the mass fragmentation around η: $w(\eta)\sim|\psi|^2$. For the scattering of two equal nuclei, the ingoing wave function would be peaked like a δ-function around the initial η-coordinate $\eta_i=0$ (see Fig. 1). After the interaction has taken place, a final mass distribution $w_f(\eta)\sim|\psi_f(t\to\infty)|^2$ emerges, where ψ_f denotes the final state wave function in the asymptotic region. The cross sections for the transfer to mass fragmentations around η are directly proportional to the probabilities $w_f(\eta)$ depicted schematically in Fig. 1. The probabilities for transferring a few nucleons are given by $w_f(\eta)$ at η values near $\eta=0$ and the transfer probabilities of larger clusters are found at $\eta\neq0$. Therefore, the fragmentation theory represents a unifying method for calculating cross sections of all reactions in which two fragments appear after the collision.

In Sect. 2 we discuss the model for fragmentation, the precise definition of the coordinates and their relation to the asymmetric two center shell model (ATCSM). In the framework of the ATCSM, using the Strutinsky formalism and the cranking model, we calculate all components of the Hamiltonian of the model. In Sect. 3 the theory is applied to explain the measured mass and charge yields in fission. The fragmentation theory can be used to predict the optimum combination of the projectile and target nuclei in order to obtain maximum fusion cross sections. This subject is discussed in Sect. 4. Finally the mass transfer in heavy ion scattering is investigated. In Sect. 5 we present realistic scattering calculations for the U+U-system and interprete the measured mass yields in the Kr+U reaction as caused by the fission of the compound nucleus.

2. Model for Fragmentation

Nucleus-nucleus collisions are complicated many-body problems. Therefore, it is necessary to reduce the degrees of freedom to those which are important and measurable. In this section, we introduce the model for fragmentations [3,4,6], which describes all two-body channels into which a compound system can decay or from which it can be formed. The main degrees of freedom of the model are the relative motion and the mass transfer between the fragments.

2.1. Collective Coordinates[6]

The cross sections of nucleus-nucleus collisions are determined by the asymp-

totic behaviour of the wave functions. The asymptotic wave functions should depend on the following collective coordinates:

a.) The relative coordinate R between the centers

b.) The mass asymmetry coordinate for two-body channels defined by the ratio

$$\eta = (A_1-A_2)/(A_1+A_2). \tag{1}$$

According to its definition the mass asymmetry coordinate is a discrete one for separated fragments and has the values $\eta=0$, $\pm\frac{2}{A}$, $\pm\frac{4}{A}$ ... with $A = A_1+A_2$ (for A even).

c.) The charge asymmetry coordinate[5] for two-body channels defined by the charge ratio $\eta_Z=(Z_1-Z_2)/(Z_1+Z_2)$. If the charge asymmetry is taken as an independent degree of freedom, the neutron asymmetry coordinate is not linearly independent because of the relation

$$\eta_N = (N_1-N_2)/(N_1+N_2) = ((A_1+A_2)\eta - (Z_1+Z_2)\eta_Z)/(N_1+N_2).$$

d.) Coordinates describing collective excitations of the fragments. For example, surface coordinates for the multipole deformations of the nuclear shape can be used in the connection with vibrator and rotator-vibrator models[7,8]. We abbreviate the sets of these coordinates by $\alpha^{(1)}$ and $\alpha^{(2)}$.

e.) Temperatures Θ_1 and Θ_2 of the fragments, which measure the statistically distributed intrinsic energies.

In the definition of the mass asymmetry coordinate a smooth transition of the asymptotically defined coordinate into the interaction region has to be required. Therefore, we introduce a plane through the neck of the compound nucleus which divides the system into two regions, as shown in Fig.2. Then, the mass asymmetry coordinate can be defined with the nuclear density as

$$\eta = \frac{1}{A}\left(\int_1 \rho d\tau - \int_2 \rho d\tau\right) \tag{2}$$

Here, we use the normalization $\int \rho d\tau = A$. The integrals are extended over region 1 or region 2, respectively. The coordinate η can be expressed as the expectation value of the corresponding operator $\hat{\eta}$ defined by:

$$\hat{\eta} = \frac{1}{A}\sum_{i=1}^{A}\left(\int_1 \delta\,(\vec{r}_i-\vec{r})\,d\tau - \int_2 \delta\,(\vec{r}_i-\vec{r})\,d\tau\right)$$

Taking the expectation value with the intrinsic many-body wave function

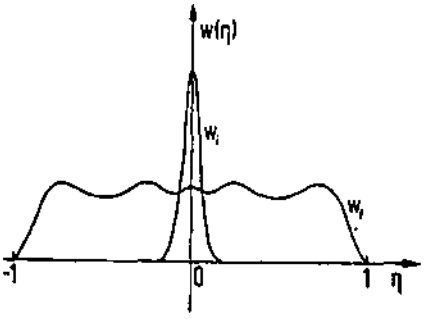

Fig. 1. Schematic picture of the probability distribution in η-space for the scattering of two equal nuclei. In the entrance channel the probability w_i is δ-peaked around η=0. The transfer cross sections are proportional to the final probability w_f, spread over the range $-1 \leq \eta \leq 1$.

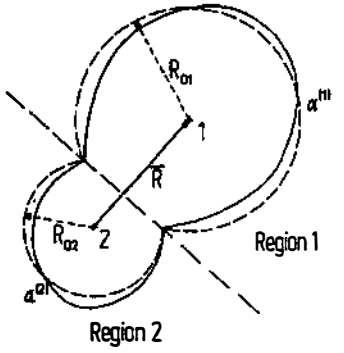

Fig. 2. Definition of the collective coordinates. The system is divided into two regions, 1 and 2, by a plane through the neck.

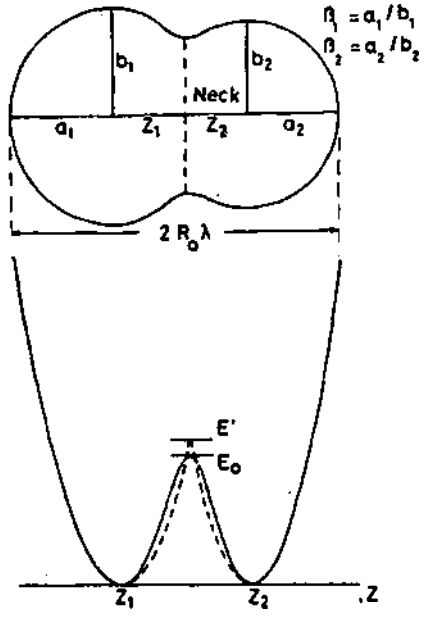

Fig. 3. The asymmetric two-center potential along the z-axis and the associated nuclear shape. The barrier heights for the definition of the neck parameter $\varepsilon = E_0/E'$ are indicated.

$\psi(\vec{r}_1 \ldots \vec{r}_A)$ we obtain the relation

$$\eta = \langle \psi | \hat{\eta} | \psi \rangle \tag{3}$$

Definition (3) is equivalent to definition (2). From the definition (2) it is evident that η is asymptotically given by discrete values, whereas in the overlap region it is a continuous coordinate. This special behaviour of the η-coordinate, i.e. discrete and continuous values depending on $\vec{R}$, introduces singularities in the transfer masses at large separations R (see Refs. 3 and 6).

If the nuclear density is assumed as homogeneous, the coordinate η approaches a coordinate ξ which is defined by the nuclear volumes V_1 and V_2 on both sides of the dividing plane:

$$\eta \to \xi = (V_1 - V_2)/(V_1 + V_2) \tag{4}$$

As long as the nuclei overlap appreciably, both coordinates η and ξ are the same: $\eta \approx \xi$.

The asymptotically defined coordinates have to be continued into the interaction region. In principle this continuation is arbitrary because the cross sections are completely determined by the asymptotic wave functions as stated above. Since we use the asymmetric two-center shell model (ATCSM) [9,10] in calculating the elements of the collective Hamiltonian, we introduce the same coordinates as chosen for the nuclear shapes in the ATCSM. In Fig. 3 a typical nuclear shape used in the ATCSM is depicted. The nuclear shapes are defined by the following set of coordinates[9]:

a.) The elongation $\lambda = (a_1 + a_2 + z_2 - z_1)/2R_o$ measures the length ℓ of the system along the symmetry axis in units of the diameter of the spherical compound nucleus: $\ell = 2R_o\lambda$.

b.) The average volume asymmetry parameter, defined by $\bar{\xi} = (a_1 b_1^2 - a_2 b_2^2)/(a_1 b_1^2 + a_2 b_2^2)$. The parameter $\bar{\xi}$ agrees only approximately with the volume asymmetry coordinate defined in Eq. (4). However, both parameters $\bar{\xi}$ and ξ are equal for separated fragments.

c.) The deformations of the fragments, which are assumed to be rotationally symmetric around the z-axis, are defined by $\beta_1 = a_1/b_1$ and $\beta_2 = a_2/b_2$.

d.) The neck parameter ε, defined by the ration $\varepsilon = E_o/E'$ where E' is the barrier height of the two-center oscillator and E_o the actual height (see Fig. 3). For $\varepsilon = 0$ a broad neck is formed, whereas for $\varepsilon = 1$ the neck has squeezed in (see Fig. 4).

e,) The thermal excitation energy E_θ, which is related to the temperature of the compound nucleus by $E_\theta = A\cdot\theta^2/10$ MeV.

When the charge asymmetry coordinate is investigated, different sets of the shape parameter of the ATCSM have to be chosen for the proton and neutron potentials. Since the potentials and, therefore, the many-body wave functions of the ATCSM depend on the volume asymmetry coordinate ξ, we obtain the mass asymmetry coordinate η by calculating the expectation value in (3) with the wave functions of the ATCSM. The result is shown in Fig. 5. In the overlap zone, characterized by $R<R_{crit}$, we find $\eta \approx \xi$ as expected, whereas in the asymptotic region ($R>R_{crit}$) the connection between η and ξ strongly depends on the prescription of how the shells of the ATCSM have been filled.

2,2. Hamiltonian

The Hamiltonian depending on the coordinates, which we have defined above, can be derived from the collective energy of the system. If we restrict ourselves to the relative motion and the mass transfer only, the energy of the system has the form:

$$H = \frac{1}{2} B_{RR}(R,\eta)\dot{R}^2 + \vec{B}_{R\eta}(R,\eta)\dot{R}\dot{\eta} + \frac{1}{2} B_{\eta\eta}(R,\eta)\dot{\eta}^2 + V(R,\eta) \qquad (5)$$

For simplification only a scalar mass B_{RR} for the relative motion is taken into account. This is not sufficient in the overlap region where a mass for the radial relative motion and a moment of inertia for the rotational motion have to be introduced. Both the masses and potentials are functions of R and η. The asymptotic mass $B_{RR}(R\to\infty,\eta)$ is the reduced mass (M=nucleon mass):

$$B_{RR}(R\to\infty,\eta) = MA_1A_2/(A_1+A_2) = MA(1-\eta^2)/4.$$

The asymptotic potential $V(R\to\infty,\eta)$ approaches the differences in binding energies:

$$V(R>>R_{crit},\eta,\eta_z) = -B(A_1,Z_1)-B(A_2,Z_2) + 2B(A/2,Z/2) + \frac{Z^2e^2}{4R}(1-\eta_z^2) \qquad (6)$$

Here, B(A,Z) is the binding energy of a nucleus with A nucleons and Z protons, and the last term is the Coulomb potential between the nuclei. In Eq. (6) we have assumed that the nuclei are in their ground states. In Sect. 5 we include the excitation energy in the potential in order to describe heavy ion scattering more realistically. As example, we consider the poten-

tial $V(R\to\infty,\eta)$ for the systems ^{40}Ca and ^{30}P in Fig. 6. The curves represent the differences in the Q-values for the various two-body break-ups of the ^{40}Ca and ^{30}P system. One recognizes the α-structures in the case of ^{40}Ca, especially the break-up into two ^{20}Ne-nuclei at $\eta = 0$.

The mass $B_{\eta\eta}$ is directly related to the velocity of the mass transfer. Let us consider the nuclear system for a fixed relative distance. Then, the energy equation of the mass transfer becomes

$$\frac{1}{2} B_{\eta\eta} \dot{\eta}^2 + V(\eta) = E_\eta \tag{7}$$

and the velocity

$$\dot{\eta} = \sqrt{2(E_\eta - V(\eta)) / B_{\eta\eta}}. \tag{8}$$

As discussed in Refs. 3 and 6 the transfer mass $B_{\eta\eta}$ is asymptotically singular at the physical discrete values of η because of $B_{\eta\eta} = B_{\xi\xi} \cdot (d\xi/d\eta)^2$ and the singularities in $d\xi/d\eta$, as shown in Fig. 5. Therefore, no transfer of nucleons asymptotically takes place between the nuclei.

The quantization of the classical Hamiltonian is carried out according to the prescription of Pauli. The classical Hamiltonian is derived from the Lagrangian L=T-V, where T and V are given in Eq.(5). Several forms of the quantized Hamiltonian are applied in the following chapters.

2.3. Calculation of Potentials and Masses

The potentials and mass parameters are calculated with the many-body wave functions of the ATCSM[9,10]. For the potentials we have used the Strutinsky method[11] in which the shell correction energies δU are added to the liquid drop energy:

$$V(R,\xi,\xi_2,\beta_1,\beta_2,\varepsilon) = V_{LDM} + \delta U \tag{9}$$

For the liquid drop model a shape of the nuclear system is chosen that agrees with the shape of the equipotential surface of the ATCSM at the nuclear surface. To obtain the dependence of the potential on the mass asymmetry coordinate η, the expectation value $\eta(\xi)$ given by Eq.(3) has to be calculated with the wave functions of the ATCSM, so that ξ can be resubstituted by η in the potential (9). In first applications of the fragmentation theory we treat only the $\vec{R}$- and η-degrees of freedom. Assuming adiabaticity for the disregarded degrees of freedom, we minimize V with respect to the de-

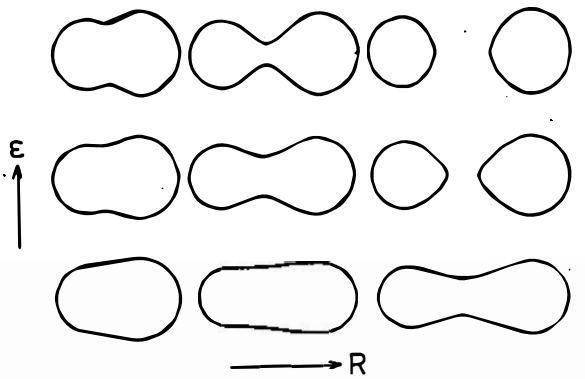

Fig. 4. Nuclear shapes in the ATCSM as functions of the two-center distance and the neck parameter.

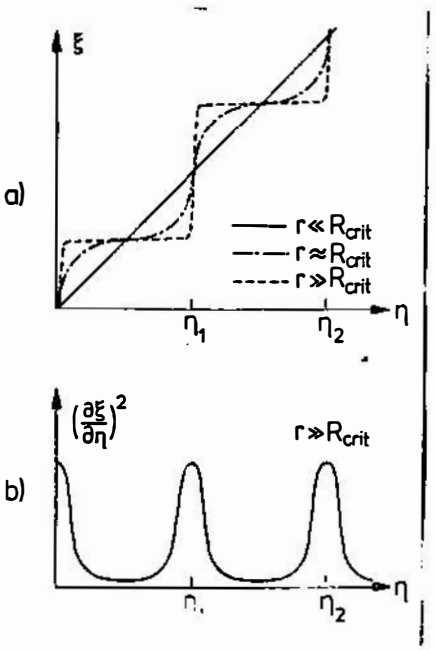

Fig. 5. The functions $\xi(\eta)$ and $(d\xi/d\eta)^2$ for two-center shell model wave functions in which always the deepest levels are occupied by the nucleons (schematically).

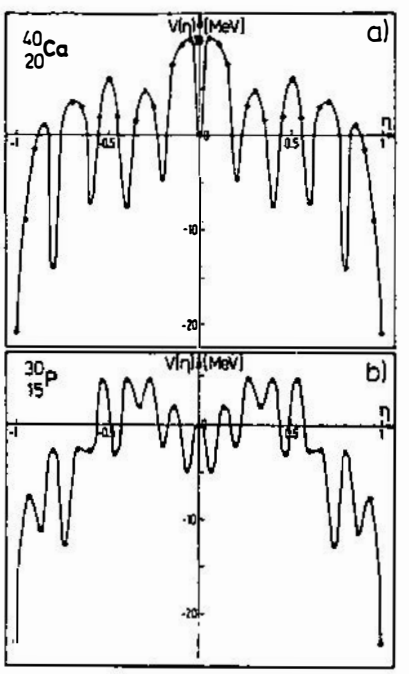

Fig. 6. The potential $V(R\to\infty,\eta)$ for the fragmentation of ^{40}Ca and ^{30}P.

formations β_1 and β_2, the neck parameter ε and the charge fragmentation coordinate η_Z, if necessary

$$V(R,\eta) = \underset{\eta_Z,\beta_1,\beta_2,\varepsilon}{\text{Min}} \; V(R,\eta,\eta_Z,\beta_1,\beta_2,\varepsilon) \tag{10}$$

The influence of the neck parameter ϵ on the potential is illustrated in Fig. 7, which presents the liquid drop energy of the compound nucleus $^{256}_{102}$No, formed in the reaction ^{48}Ca + ^{208}Pb. The liquid drop energy is drawn as function of ε for various lengths of the compound nucleus. Between the inner minimum at $\varepsilon = 0$, where no neck is formed, and the outer minimum at $\varepsilon > 1$, where already a neck has been built up, a barrier exists up to a length of $\ell = 24$ fm. In a scattering experiment the nuclei run along the indicated path and overcome the barrier at lengths $\ell < 24$ fm, where they gain about 40 MeV energy by filling out the neck. This is a sudden process. The fission of the compound system occurs along the minimum valley at $\varepsilon=0$ without necking-in. Only at values $\ell > 34$ fm the fissioning system has a rapid transition to separated nuclear shapes. Therefore, two channels exist with $\varepsilon \approx 0$ and $\varepsilon > 1$, which may be denoted as the fission channel and scattering channel.

Fig. 8 gives an impression of the deformation effects which happen during a collision of ^{238}U on ^{238}U in the symmetric channel[12]. The potential energy surface depends on the two center distance Δz and a parameter h measuring the neck (no neck for h=0). The dashed line represents a possible way for the approach of the nuclei and the dotted-dashed line is the way along which the fission process runs. Fig. 9 shows the shapes of the U+U-system going together on the dashed line and getting away on the dotted-dashed line. From these pictures it is evident that the deformations and the neck parameter have to be included as dynamical degrees of freedom in a theory of fragmentation.

The masses in the kinetic energy of Eq. (5) can be consistently calculated by applying the cranking model and the same ATCSM-states as used for determining the shell corrections δU to the liquid drop energy in Eq. (9). The cranking masses are given by the formula

$$B_{ij} = -2\hbar^2 \sum_{n\neq o} \frac{\langle \Phi_o | \frac{\partial}{\partial \beta_i} | \Phi_n \rangle \langle \Phi_n | \frac{\partial}{\partial \beta_j} | \Phi_o \rangle}{E_n - E_o} \tag{11}$$

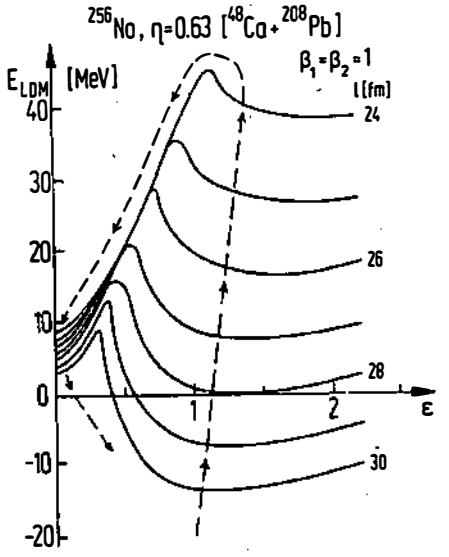

Fig. 7. The liquid drop potential for $^{48}Ca + ^{208}Pb \rightarrow ^{256}No$ ($\eta = 0{,}63$) as function of the neck parameter ε

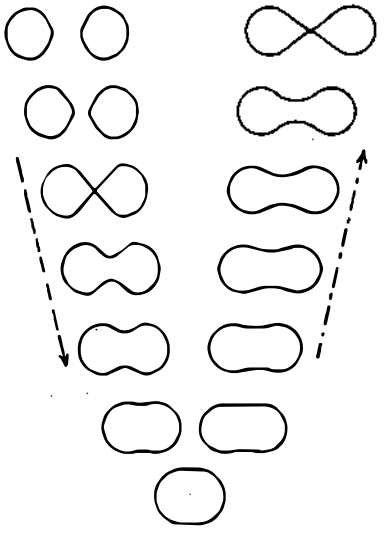

Fig. 9. Nuclear shapes for the approach and fission of the ^{238}U-^{238}U system.

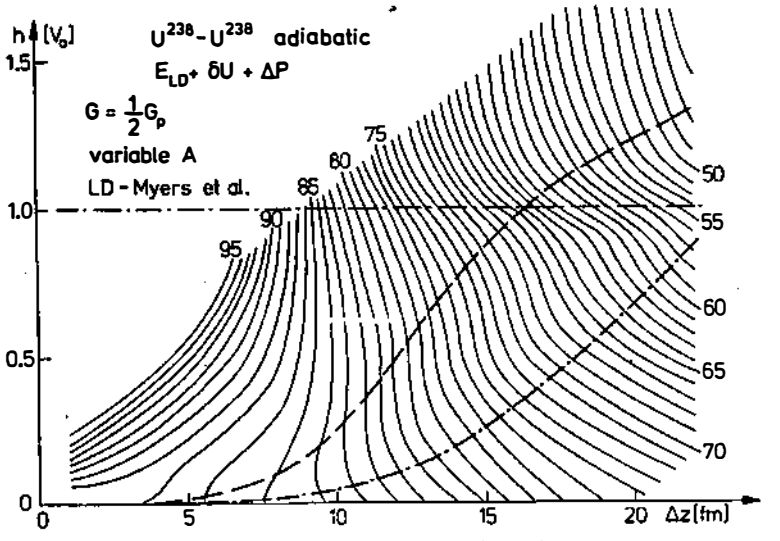

Fig. 8. The potential energy surface for ^{238}U-^{238}U. The distance between the two centers is denoted by Δz and the neck parameter by $h=E_o/V_o$ with the barrier height E_o and the potential V_o at the nuclear surface (from (Ref.12). Lines along the gradient are drawn which represent the scattering and fission paths.

The coordinates β_i are the collective coordinates introduced above, on which the many-body wave functions ϕ_n of the ATCSM depend. The ground-state function is denoted by ϕ_o and the wave functions of the excited states by ϕ_n. In actual calculations pairing is taken into account which leads to a slightly different formula in the BCS formalism. As discussed in Refs. 13 and 14 the essential assumption of the cranking model, the adiabaticity assumption, may be questioned for the relative motion in heavy ion collisions. Therefore, non-adiabatic cranking models as developed in Ref. 13 have to be applied. For the mass transfer the adiabaticity assumption seems to be correct, because the mass transfer is a slow process compared with the relative motion in nucleus-nucleus encounters.

3. Mass and Charge Fragmentation in Fission

In the following we review the calculations of the mass and charge yields of fissioning nuclei [4,5,15], using the fragmentation theory in the framework of the ATCSM.

3.1. Formalism for Mass and Charge Fragmentation

Because the mass and charge fragmentation is already fixed before the scission point, one can use the volume asymmetry coordinate ξ instead of η. Further we assume the adiabatic approximation that both the ξ- and ξ_Z-motions are fast compared to the relative motion. The reason is, that for the spontaneous fission and for the fission under the barrier the relative motion described by λ is slow after the system has tunnelled through the barrier and has first begun to run down the Coulomb potential to the scission point. Furthermore, the potential $V(\lambda,\xi)$ remains nearly unchanged in its dependence on the asymmetry coordinates ξ and ξ_Z at later stages of λ (see Fig. 16), so that the mass and charge distributions are already fixed at λ-values just after the penetration of the barrier. Assuming complete adiabaticity we can regard λ as a time-independent parameter and obtain the stationary Schrödinger equation in ξ by quantizing Eq.(5), where R and η are replaced by λ and ξ:

$$\left(\frac{-\hbar^2}{2\sqrt{B_{\xi\xi}(\lambda,\xi)}}\frac{\partial}{\partial\xi}\frac{1}{\sqrt{B_{\xi\xi}(\lambda,\xi)}}\frac{\partial}{\partial\xi} + V(\lambda,\xi) - E_\lambda^{(\nu)}\right)\psi_\lambda^{(\nu)}(\xi) = 0 \qquad (12)$$

The states $\psi_\lambda^{(\nu)}$ are vibrational states in the potential V and classified by the quantum numbers $\nu = 0, 1, 2 \ldots$. An analogeous equation can be formulated for the charge asymmetry coordinate ξ_Z for fixed values of λ and ξ. In the calculation of the potential $V(\lambda,\xi)$ the Strutinsky formalism has

been applied by using the single particle energies of the ATCSM and the liquid drop model of Myers and Swiatecki[16]. The potential is minimized with respect to the neck parameter ε and the deformation parameters β_1 and β_2. Then the parameters ε, β_1 and β_2 on which the single particle wave functions depend become functions of λ and ξ. This λ- and ξ-dependence has the consequence that in the calculation of the collective mass parameters $B_{\xi\xi}$, $B_{\lambda\xi}$ and $B_{\lambda\lambda}$ with the cranking formula (11) the derivatives of ε, β_1 and β_2 with respect to λ and ξ have to be taken into account.

In spontaneous fission, starting from the nuclear ground state, only the lowest vibrational state $\nu=0$ of Eq. (12) may be occupied. However, for fission from excited states and because of the interaction between the λ- and ξ-degrees of freedom, higher states $\psi_\lambda^{(\nu)}$ become excited. In most applications a nuclear temperature Θ is introduced and a Boltzmann-like occupation of the excited states is assumed:

$$|\psi_\lambda|^2 = \sum_{\nu=0}^{\infty} |\psi_\lambda^{(\nu)}|^2 \exp\left(-E_\lambda^{(\nu)}/\Theta\right) \quad . \tag{13}$$

In a more complete treatment of the nuclear-temperature effects, one has to regard also the temperature in the potentials and cranking masses assuming a Fermi-distribution for the occupation of the ATCSM-states (see Brack et al.[11]). The probability of finding a certain mass (or charge) fragmentation ξ(or ξ_Z) at a position λ on the fission path is proportional to $|\psi_\lambda|^2$. For mass distributions this probability is scaled to the mass yield at a mass number A_1 of one fragment ($d\xi = 2/A$, in percent):

$$Y(A_1) = 2|\psi_\lambda\ (\xi(A_1))|^2 \ \sqrt{B_{\xi\xi}(A_1)}\ \frac{2}{A}\ 100 \tag{14}$$

The analogous formula, where ξ is replaced by ξ_Z, gives the fractional charge yields $Y(Z_1)$ at a charge number Z_1. Both these yields are directly comparable with experiments.

3.2. Comparison with Experiments

According to the method described in Sect. 3.1., mass-yield distributions have been calculated[4] for the fission of ^{226}Ra, ^{236}U and ^{258}Fm, which are typical examples of triple-, double- and single-humped mass distributions.

Asymmetric fission:The fission of ^{236}U produces an asymmetric mass distribution, as shown in Fig. 1o. The calculations of the masses and potentials are done for the value of λ=1.8 and depicted in Fig. 1o. Whereas the potential

is rather smooth with asymmetric minima around A=140 and 96 corresponding to $|\varepsilon| \approx 0.2$, the mass parameters exhibit rapid oscillations. Fig. 13 shows the nuclear shape for $\lambda=1.8$ at the point of the minima of the potential energy. The experimental data[17] are measured in thermal neutron fission of ^{235}U and, therefore, correspond to an excitation energy of ^{236}U of about 6 MeV. The calculated distributions give a semi-quantitative agreement with experiment. The peaks are somewhat too narrow and the valley is too low for the ground state (Θ=0) but the picture improves as excitation is introduced into the system.

Triple-humped fission: For ^{226}Ra the potential has three minima which are responsible for the triple-humped mass yield. In Fig. 11 we compare the calculated mass yield with the measured mass yield of ^{227}Ac obtained from the fission of ^{226}Ra with 11MeV protons[18]. Although the three potential minima are equal in depth for $\lambda=1.8$, the mass distribution has a lower peak in the middle because of the rather small mass parameter $B_{\varepsilon\varepsilon}$ in that region.

Symmetric fission: The nucleus ^{258}Fm is an example for symmetric fission as demonstrated in Fig. 12. The calculations are qualitatively similar to the mass yield observed in thermal neutron fission of ^{257}Fm[19].

Charge distributions are calculated[5] for the mass fragmentations $|\varepsilon|=0.195$ and 0.20 of ^{236}U which refer approximately to the mass chains $A_1=141$, $A_2=95$ and $A_1=142$, $A_2=94$. Fig. 13 shows the set of the parameters used in the definition of the ATCSM-potentials for the protons and neutrons. Fig.14 gives the calculated potential energy and the mass parameters for $\varepsilon = \pm 0.195$ and $\lambda=1.8$. We obtain the interesting result that the potentials show single deep minima at $\varepsilon_Z = \pm 0.195$. Because of $\varepsilon = \varepsilon_Z = \varepsilon_N$ at the minima the hypothesis of an unchanged charge distribution is supported in this example. Fig. 15 compares the calculated and experimental charge dispersion yields for both $|\varepsilon| = 0.195$ and 0.20. The experimental data[20] correspond to the mass chains with $A_1=141$ and 142. The calculated charge dispersion curves have Gaussian functional form peaked around Z=55 and 55.2 and have widths of the order of the experimental values. The calculations refer to the spontaneous fission without taking into account the evaporation of neutrons. Newer measurements on charge distributions in light mass chains have revealed the role of pairing and odd-even effects[21].

It should be kept in mind that in all the above calculations not a single parameter is fitted to yield the experimental distributions. The calcula-

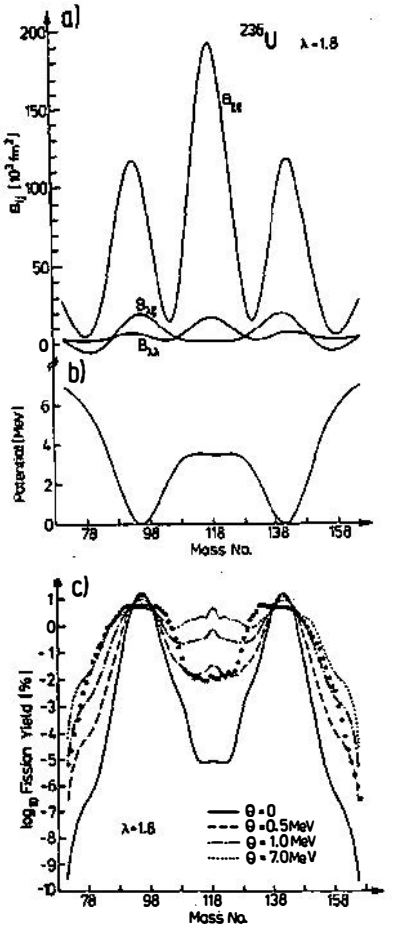

Fig. 10. The mass yield for ^{236}U-fission at λ = 1.8.
a.) mass parameters in units of the nucleon mass,
b.) the potential energy,
c.) comparison of the theoretical mass yields for various temperatures with the experimental data, taken from Ref. 17.

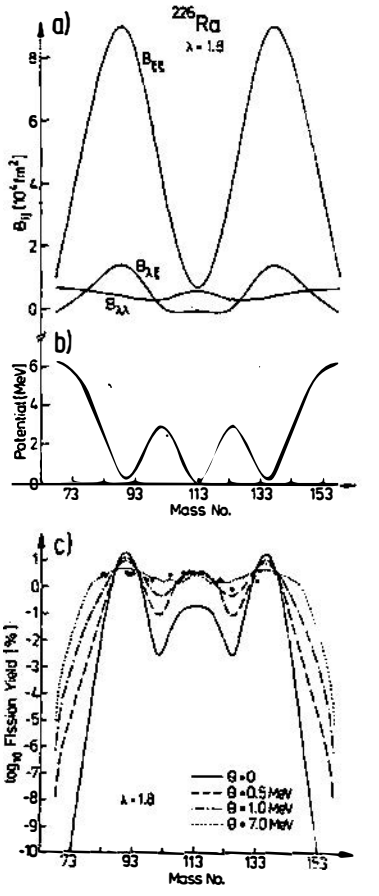

Fig. 11. The mass parameters, the potential energy, the theoretical and experimental mass yields for ^{226}Ra-fission at λ = 1.8. The experimental data are taken from Ref. 18.

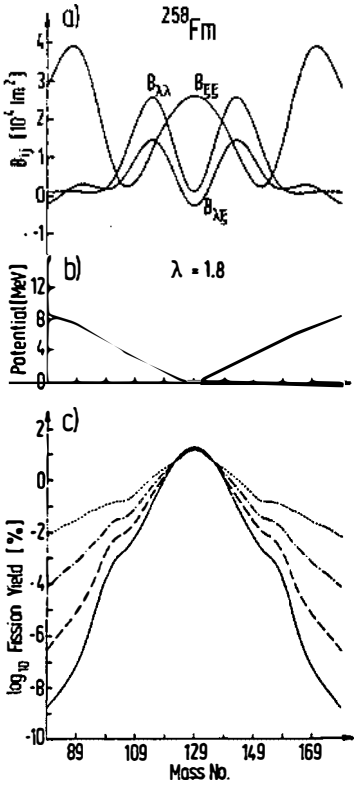

Fig. 12. The mass parameters, the potential energy and mass yields for ^{257}Fm-fission at λ = 1.8. The temperatures are o, o.5, o.75 and 1.25 MeV.

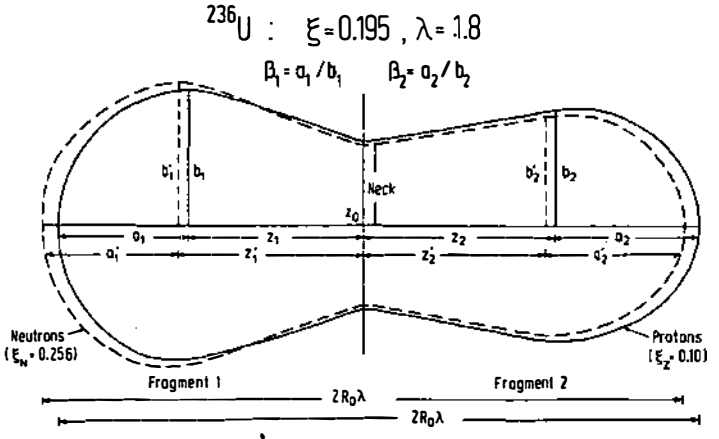

Fig. 13. The parameters of the ATCSM used in the calculation of the charge dispersion. Different potentials for the protons and neutrons are assumed.

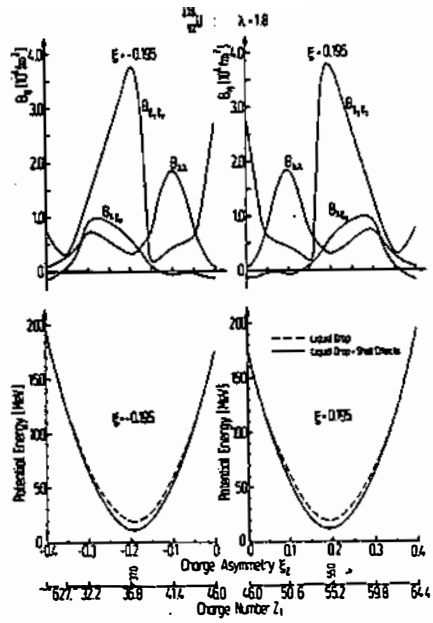

Fig. 14. Mass parameters and potential for the charge fragmentation for $\xi = \pm 0.195$ in the fission of ^{236}U at the elongation $\lambda = 1.8$.

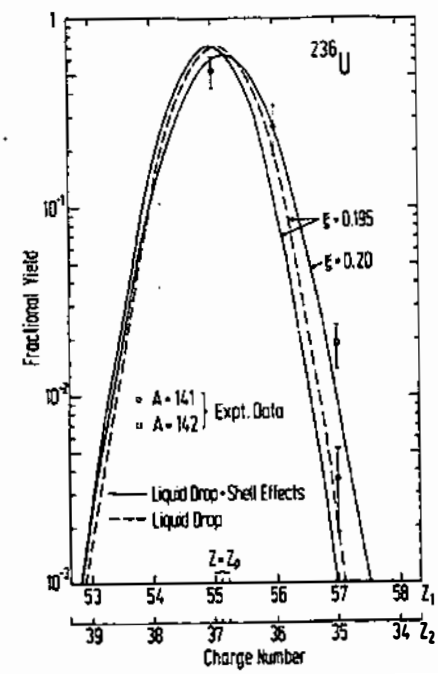

Fig. 15. Calculated charge dispersion curves for the mass asymmetries $|\xi| = 0.195$ (A_1=141) and 0.20 (A_1=142) in the fission of ^{236}U at the elongation $\lambda = 1.8$. The experimental data are taken from Ref. 20.

tions show that both the mass- and charge-distributions are fixed mainly by the potential energy surfaces whereas the mass parameters determine the details, e.g. the peak-to-valley ratio.

3.3 Time-Dependent Treatment of the Elongation[15]

In this section we take the relative motion of the nascent fragments and its interaction with the mass asymmetry vibrations into account. For this we start with the classical total energy of the system

$$H(\lambda,\xi) = \frac{1}{2} B_{\lambda\lambda} \dot{\lambda}^2 + B_{\lambda\xi} \dot{\lambda}\dot{\xi} + \frac{1}{2} B_{\xi\xi} \dot{\xi}^2 + V(\lambda,\xi) \tag{15}$$

It is assumed that the elongation can be described by the classical time-dependent coordinate $\lambda(t)$ whereas the motion in the fragmentation coordinate ξ is quantized. Therefore, a semi-classical formalism is set up in which the wave function $\psi(\xi,t)$ is the solution of the time-dependent Schrödinger equation with $\lambda(t)$.

$$i\hbar \frac{\partial}{\partial t} \psi = \{ - \frac{\hbar^2}{2\sqrt{B_{\xi\xi}(\xi,\lambda(t))}} \frac{\partial}{\partial \xi} \frac{1}{\sqrt{B_{\xi\xi}(\xi,\lambda(t))}} \frac{\partial}{\partial \xi} + V(\xi,\lambda(t)) \} \psi \tag{16}$$

In Eq. (16) we have neglected the terms arising by the coupling mass $B_{\lambda\xi}$ in (15). This is justified because of $|B_{\lambda\xi}| << \sqrt{B_{\lambda\lambda} B_{\xi\xi}}$ in all actual problems (see Figs. 10-12). The solutions of (16) are expanded in the stationary eigen functions of Eq. (12):

$$\psi(\xi,t) = \sum_{\nu=0}^{\infty} a_\nu(t) \, \psi^{(\nu)}_{\lambda(t)}(\xi) \exp\left(-\frac{i}{\hbar} \int_0^t E^{(\nu)}_{\lambda(t')} dt'\right) \tag{17}$$

The classical equation of motion for λ is obtained by calculating the average value of the energy (15) with the wave function (17) and neglecting again the coupling mass $B_{\lambda\xi}$:

$$E_{av} = \frac{1}{2} < B_{\lambda\lambda} > \dot{\lambda}^2 + \sum_{\nu=0}^{\infty} |a_\nu|^2 E^{(\nu)}_\lambda \tag{18}$$

In order to estimate the possible effects of energy dissipation into single-particle degrees of freedom a parametrized frictional force is included. Then the equation of motion for λ is given by

$$\frac{dE_{av}}{dt} = - f \dot{\lambda}^2 , \tag{19}$$

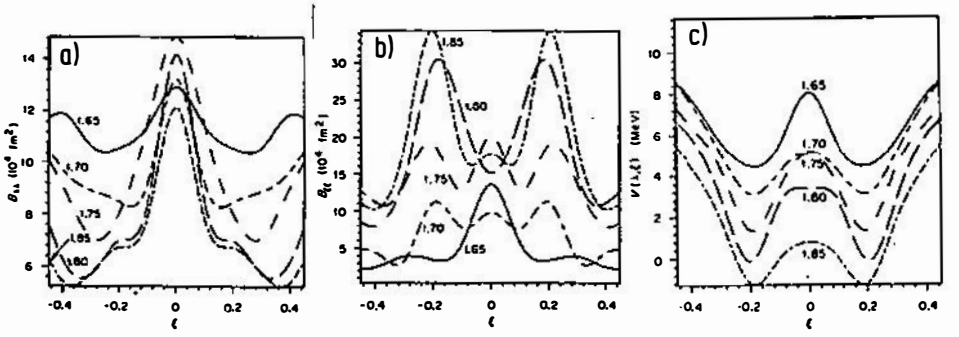

Fig. 16. The mass parameters $B_{\lambda\lambda}$ and $B_{\xi\xi}$ and the potential V for ^{236}U for various values of the elongation λ as indicated at the curves.

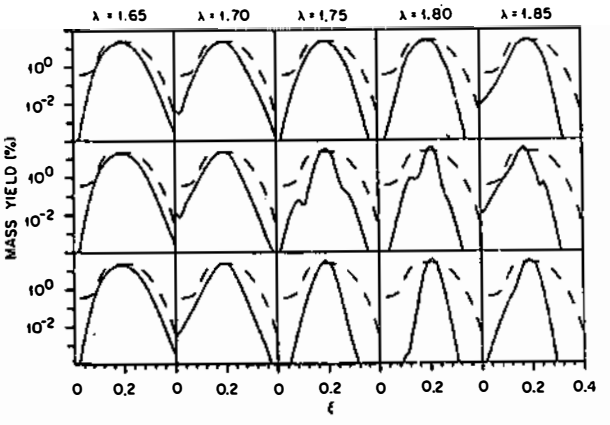

Fig. 17. The collective wave functions, converted to an equivalent mass yield of ^{236}U. Each row shows the development of the wave function in a particular case. The top row is for friction f=o, the middle one for $f=1o^{-18}$MeV sec, and the bottom one for $f=4\cdot1o^{-18}$MeV sec.

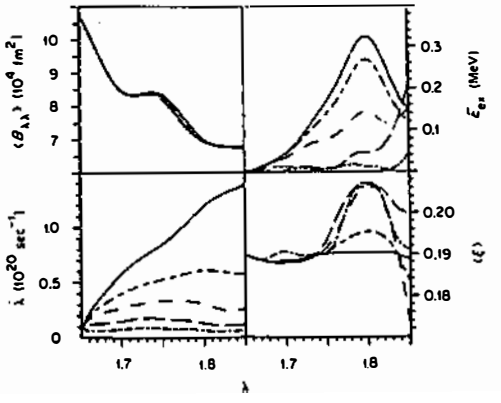

Fig. 18. Results of the dynamical calculation for ^{236}U: average mass parameter $\langle B_{\lambda\lambda}\rangle$, elongation velocity $\dot{\lambda}$, collective excitation energy E_{ex} and average mass asymmetry $\langle\xi\rangle$. The various curves correspond to the friction constants f=o,5,1o,2o and $4o\cdot1o^{-19}$MeV sec.

where f is the coefficient of friction. The classical equation of motion for $\lambda(t)$ is simultaneously solved together with the time-dependent Schrödinger equation (16). As initial condition we have chosen $\dot{\lambda} = 0$ for the λ-value after the system has finished tunneling through the barrier.

The calculations are done for the fission of ^{236}U with the masses and potentials shown in Fig. 16. The system starts at $\lambda = 1.65$ which is the exit point of the system after tunneling in spontaneous fission. Figs. 17 and 18 present the results for the dynamical development of the wave function for several values of the friction coefficient f, which were chosen such that the transition from unimpeded acceleration to very slow motion can be studied. The collective excitation energy has been defined as $E_{ex} = \sum_{\nu} |a_\nu|^2 (E^{(\nu)} - E^{(o)})$ and the mean asymmetry coordinate as $\langle\xi\rangle = \sum_{\nu,\mu} a_\nu^* a_\mu \langle\nu||\xi||\mu\rangle$. For no friction the mass yield in Fig. 17 changes little and is close to the sudden case while for very strong friction and slow descent it adopts adiabatically. The intermediate cases show some oscillations which are due to coherent excitation of higher ξ-states.

We conclude that any detailed study of the peak-to-valley ratio and the structure of the mass yields will not be possible without studying dynamics. Fissioning nuclei which have intermediate velocities in the elongation would reveal oscillations in the mass yield caused by the excitation of higher vibrational states in the asymmetry coordinate. Such effects have not yet been observed in experiment.

4. Production of New Elements in Fusion Reactions

The fragmentation theory can be applied to select the proper target and projectile combinations for producing superheavy elements in fusion reactions through heavy ion collisions. The production cross sections are shown to be very sensitive to the choice of the reaction partners. The Berkeley group[22] has bombarded spherical, light projectiles on deformed, heavy targets, whereas the Dubna group[23] has used spherical or nearly spherical but relatively heavier projectiles on deformed and spherical heavy targets. Different isotopes of heavy elements with Z = 102-106 have been synthesized by these two groups. In the following we investigate the question of the optimum choice of the reaction partners.

The idea of the method suggested in Ref. 24 is to choose the reaction partners such that the compound system is formed with a minimum of excitation energy. For a cooler compound nucleus, the number of neutrons emitted would

be smaller and consequently the cross section for the formation of the nucleus in the ground state would be large. The compound system can be reached by various combinations of the projectile and target nucleus. As we shall see, the potential energy $V(R,\eta,\eta_Z)$ of the system already gives sufficient information for qualitative conclusions about the probability of forming a cool compound nucleus.

Fig. 19 shows the potential $V(R,\eta)$ for the compound nuclei $^{258}_{104}$ and $^{260}_{106}$. In the overlap zone ($R<R_c$) we have carried out a full three dimensional minimization in ε, β_1, β_2 and in the asymptotic region ($R>R_c$) we have used Eq. (6) minimizing $V(R,\eta,\eta_Z)$ for each possible combination of masses and charges. The binding energies in Eq. (6) are taken from the atomic mass tables of Seeger[25]. We notice from Fig. 19 that for each compound nucleus deep minima in the potential energy occur at only a few η-values. The interesting point is that these deep minima in $V(R,\eta)$ are not only stable in η, but also that no new minima appear after the two nuclei overlap to form the compound system. Therefore, the potential $V(R = R_c,\eta,\eta_Z)$, which is easily computable through Eq. (6), gives already the positions of the minima with respect to η and η_Z. Evidently, the potential minima in Fig. 19 are related to shell effects, with at least one of the two nuclei being a spherical nucleus. This fact is demonstrated in Fig. 19 where the static deformations β_1 and β_2, taken from Ref. 25, are plotted for $R = R_c$.

The collective Hamiltonian couples the surface vibrations and the mass- and charge-fragmentation degrees of freedom strongly. When the transfer of mass and charge occurs, the shapes of the two incoming nuclei change, which apparently causes a large transfer of energy into the surface degrees of freedom. Two different cases of initial fragmentation can be distinguished which lead to a different amount of excitation of the compound system: 1.) the initial fragments lie outside the potential energy minima of Fig. 19 and are non-spherical, 2.) the initial fragments lie on the energy minima in which case either one or both nuclei are spherical. In case 1.), a large mass and charge transfer occurs in the direction to the minima of the potential $V(\eta)$ because the driving forces, given by $-\partial V/\partial\eta$ and $-\partial V/\partial\eta_Z$, act on the system. While the system runs in the direction to the potential minima, a large amount of energy is transferred into the excitation of surface vibrations. On the other hand, in case 2.), no mass and charge transfer occurs since the driving forces $-\partial V/\partial\eta$ and $-\partial V/\partial\eta_Z$ vanish in the potential minima.

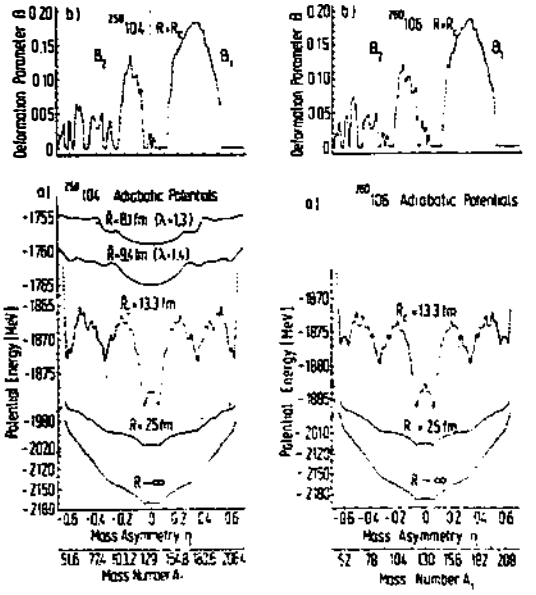

Fig. 19.
a,) Potential energy as function of η and R for the compound systems $^{258}_{104}$ and $^{260}_{106}$.
b.) Deformation parameters for R = R_c.

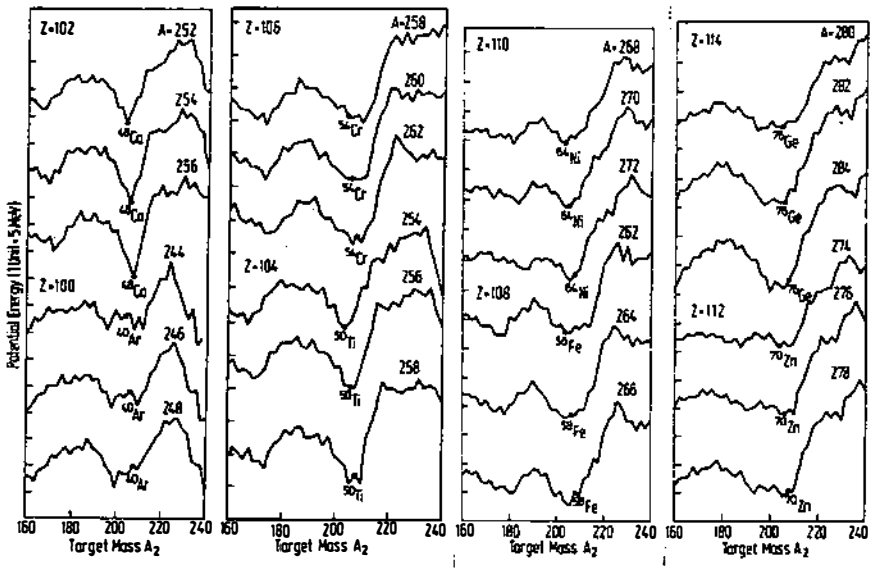

Fig. 2o. Potential energy as a function of the target mass A_2 at the critical distance $R=R_c$ for various compound masses (A) with $100 \leq Z \leq 114$. The targets are Pb-nuclei. Several projectile nuclei are indicated.

We find, therefore, that the excitation of the compound nucleus would be minimum if the target and projectile are chosen with respect to the minima in the potential $V(R,\eta,\eta_Z)$ and further if the compound system is formed in a central collision. As a first test of this selection rule we consider the minima of the potentials in Fig. 19 which are listed in tables by Gupta[3] and Sandulescu et al.[24]. It is interesting to find that the combinations $^{5o}_{22}Ti + ^{2o6}_{82}Pb$, $^{5o}_{22}Ti + ^{2o8}_{82}Pb$ and $^{54}_{24}Cr + ^{2o6}_{82}Pb$ are used in Dubna-experiments for the synthesis of Z = 1o4 and 1o6 elements (for references see Gupta[3]).

Fig. 2o presents calculations[26] of the potential energy at the relative distance $R=R_c$ for the case that the target is a Pb-nucleus and the compound nucleus is a heavy or superheavy element with 1oo ≤ Z ≤ 114 protons. The success of the theory is again shown in the case of Z = 1oo, where ^{4o}Ar projectiles have already been used for the synthesis of Fm isotopes. The theory suggests ^{58}Fe, ^{64}Ni, ^{7o}Zn and ^{76}Ge for the synthesis of the superheavy elements 1o8, 11o, 112 and 114 in the compound nucleus reactions with Pb-targets.

The selection of the target and projectile combinations according to the minima of the potential $V(R,\eta,\eta_Z)$ is a necessary condition to obtain large fusion cross sections. Further conditions are large mass- and charge- asymmetries, large interaction radii and small interaction barriers as pointed out by Gupta et al.[27].

5. Mass Transfer in Heavy Ion Scattering

The fragmentation theory can be applied to the scattering of nuclei. Here we discuss the mass transfer in the collision $^{238}U - ^{238}U$ and the quasi-fission process in the reaction of ^{84}Kr ions with ^{238}U.

5.1. Mass Transfer in the $^{238}U - ^{238}U$ Collision[28]

The fragmentation theory assumes that the collisions of two nuclei can be described by the coordinate $\vec{R}$ of the relative motion and by the fragmentation coordinate η defined in Eq. (1). The energy of the system has the following form:

$$H = \frac{1}{2} B_{RR}(R,\eta)\, \dot{\vec{R}}^2 + \vec{B}_{R\eta}\, \dot{\vec{R}}\dot{\eta} + \frac{1}{2} B_{\eta\eta}\, \dot{\eta}^2 + V(R,\eta,\theta) + \tilde{E}(\theta) \qquad (2o)$$

The first three terms denote the kinetic energy, $V(R,\eta,\theta)$ is the potential and $\tilde{E}(\theta)$ the energy transferred out of the $\vec{R}$- and η-motion into the degrees of freedom which are not treated explicitely. In order to simplify the calculations, the coupling term in (2o) is neglected because of $|\vec{B}_{R\eta}| << \sqrt{B_{RR} \cdot B_{\eta\eta}}$.

The masses calculated by Zohni[29] have large fluctuations as function of η. Since these fluctuations are strongly dependent on the underlying cranking and shell models, we have used masses averaged over the masses of Ref. 29. The averaged masses are plotted in Fig. 21.

a.) The temperature-dependent potential: The potential V and the energy loss $\tilde{E}$ in the $\vec{R}$- and η- motion are assumed to depend on the temperature θ of the compound system. We use the ansatz:

$$V(R,\eta,\theta) = V_{LDM}(R,\eta) + e^{-(\theta/\theta_o)^2}\Delta V_{shell} \qquad (21)$$

The potential V_{LDM} is the liquid drop energy as function of the coordinates R and η. The difference ΔV_{shell} represents the shell effects in the adiabatic potential. Fig. 22 shows the adiabatic fragmentation potentials of the $^{238}U + ^{238}U$-system by solid lines at several internuclear distances. The potentials were calculated by Zohni[29] within the Strutinsky formalism and the ATCSM. At the potential minimum at η = 0.118 one of the partners is a Pb-nucleus and at the minimum at η = 0.28 superheavy nuclei with Z ≈ 118 are formed. The dashed curves in Fig. 22 give the liquid drop potentials V_{LDM} used in Eq. (21).

The shell effects in the adiabatic potential are smoothed out with the exponential factor in Eq. (21). According to Ref. 30 the shell effects vanish above an excitation energy of 60 MeV in the Uranium region, corresponding to a temperature of about θ_o=1.5 MeV. The same transition temperature is used for the compound nucleus A=476 which corresponds to an excitation energy of about E_o=100 MeV above which the shell effects vanish.

b.) The excitation energy: The energy $\tilde{E}$, which is lost in the $\vec{R}$- and η-motion, may be devided up into three parts: 1.) the statistically distributed thermal excitation energy E_θ which is related to the temperature θ of the compound system, 2.) the excitation energy E_c of the collective degrees of freedom, which are not explicitly treated, like surface vibrations and 3.) the exitation energy E_{sp} transferred into single particle degrees of freedom via direct reactions, e.g. into the prompt emission of nucleons.

$$\tilde{E} = E_\theta + E_c + E_{sp} \qquad (22)$$

It is assumed that the excitation of collective vibrations and the direct emission of a few nucleons do not smooth out the shell effects in the adia-

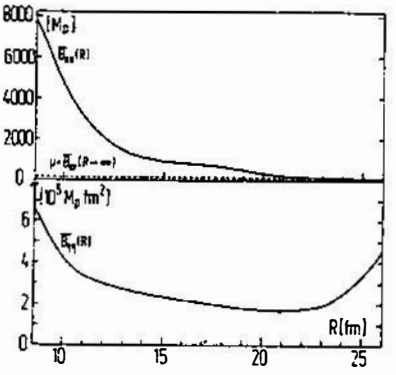

Fig. 21. The masses $\bar{B}_{RR}(R)$ and $\bar{B}_{\eta\eta}(R)$ averaged over the η-coordinate for A=476.

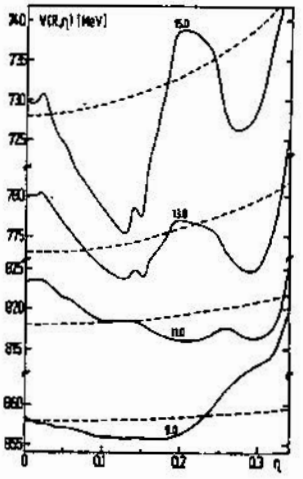

Fig. 22. The fragmentation potential for A=476 for various relative distances. The solid lines are the adiabatic potentials. The dashed lines show the liquid drop model potentials V_{LDM}.

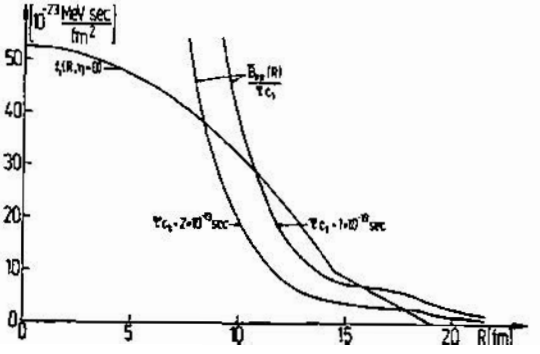

Fig. 23. The radial friction function $f_1(R)$ for ^{238}U-^{238}U defined in Ref. 31. Also the function $\bar{B}_{RR}/\bar{\tau}c_1$ is shown.

batic potential. In order to fix the thermal energy, we introduce the sharing parameter f which determines the percentage of the thermal excitation energy in the total excitation energy

$$E_\Theta = f \tilde{E}. \tag{23}$$

The sharing parameter f is considered as a free parameter since no ab-initio calculations of f presently exist. The statistically excited degrees of freedom are assumed to be in thermodynamical equilibrium with temperature Θ. Therefore, we can use the relation (Θ in MeV):

$$E_\Theta = A\Theta^2 \,/\, 10 \text{ MeV} \tag{24}$$

With Eq. (24) the temperature-dependence of the exponential factor in (21) may be replaced by its dependence on the excitation energy:

$$V = V_{LDM}(R,\eta) + e^{-f\tilde{E}/E_o}\, \Delta V_{shell}, \tag{25}$$

where E_o is given by $E_o = A\Theta_o^2 \,/\, 10$ MeV.

All the degrees of freedom which are not explicitly treated and which carry the total excitation energy $\tilde{E}$, are assumed to couple to the relative motion and mass transfer via the friction. To simplify the further investigations we take only the radial friction into account and, therefore, write the excitation energy $\tilde{E}$ at time t as follows:

$$\tilde{E}(t) = c_1 \int_{-\infty}^{t} f_1\,(R,\eta)\, \dot{R}^2\, dt' \tag{26}$$

The radial friction $c_1 f_1 \dot{R}$ is taken from Ref. 31 and shown in Fig. 23. An analysis[28] of the cranking model yields a relation between the cranking mass and friction function. Assuming an average decay time $\bar{\tau}/2$ for the decay of the excited 1-particle-1-hole-states of the cranking model into more complex states we obtain the energy dissipation as:

$$\tilde{E}(t) = \int_{o}^{t} \frac{\bar{B}_{RR}}{2}\, \dot{R}^2\, \frac{dt'}{\bar{\tau}/2} \tag{27}$$

By comparing Eqs. (26) and (27) a simple connection follows: $\bar{B}_{RR}/\bar{\tau} = c_1 f_1(R)$. In Fig. 23 we have fitted the expression $\bar{B}_{RR}/\bar{\tau}c_1$ to the friction function and find $\bar{\tau}c_1 = 1 - 2 \cdot 10^{-19}$ sec which yields realistic decay times of $\bar{\tau} \approx 10^{-21}$ sec with $c_1 = 50 - 200$ for the dissipation of energy.

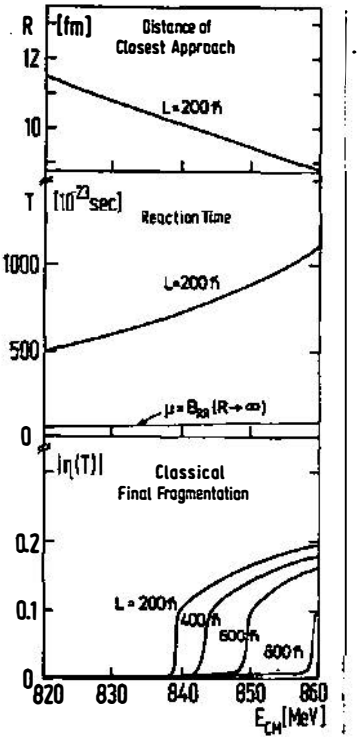

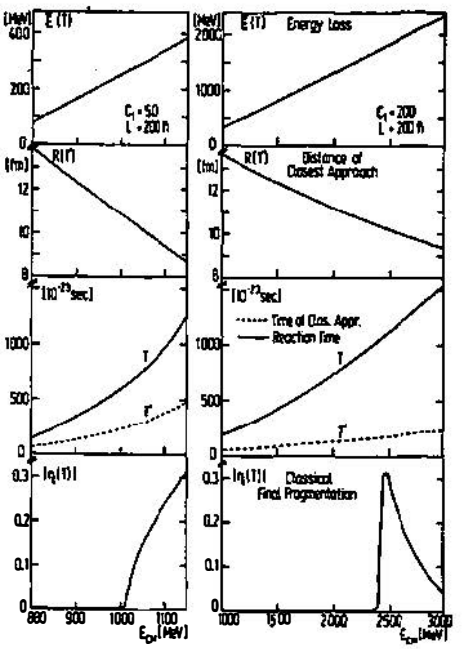

Fig. 25. The same quantities as in Fig. 24 calculated with friction and f = 0.

Fig. 24. Results of the classical calculations without friction for the ^{238}U-^{238}U collision. The distance of closest approach, the reaction time and the mass fragmentation as function of the incident energy E_{CM}.

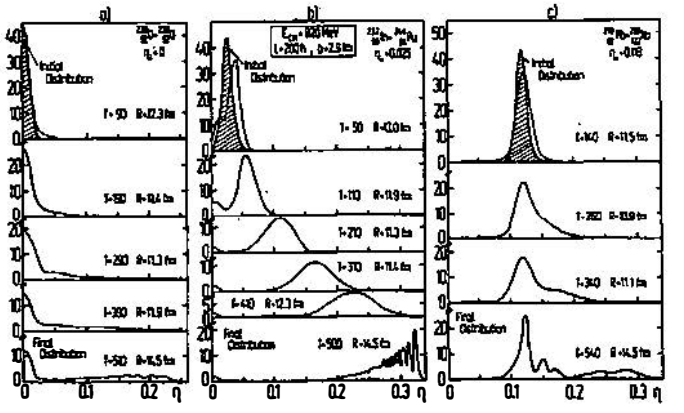

Fig. 26. The time evolution of the mass fragmentation without friction for different initial distributions η_i. The times are given in units of 10^{-23}sec.

c.) Results with the classical equations of motion: In order to study the time evolution of the fragmentation we first determine the classical time dependence of the relative motion and fragmentation coordinate. For this we solve the equations of motions which are derived from the Hamiltonian of the system.

$$H = \frac{p_R^2}{2B_{RR}} + \frac{L^2}{2B_{RR}R^2} + \frac{p_\eta^2}{2B_{\eta\eta}} + V(R,\eta,\tilde{E}) + \tilde{E} \qquad (28)$$

Here, $\vec{L}$ is the orbital angular momentum, $p_R = B_{RR}\dot{R}$ the relative momentum and $p_\eta = B_{\eta\eta}\dot{\eta}$ the momentum of the fragmentation degree of freedom. Solving the coupled equations of motions following from Eq.(28) we obtain the time-dependent functions $R(t)$, $p_R(t)$, $\eta(t)$ and $p_\eta(t)$.

In Fig. 24 we study the U-U collision without friction in the adiabatic potential $V_{ad}(R,\eta) = V(R,\eta,0 = 0)$. We present the distance of closest approach, the reaction time and the classical final fragmentation, obtained as solutions of the classical coupled equations. The classical mass fragmentation corresponds to the expectation value of the fragmentation distribution. It is hindered by the existence of the small barrier at $\eta = 0.02$ in the potential of Fig. 22. As the incident energy increases, the distance of closest approach decreases. When the distance of closest approach becomes smaller than 10.2 fm, the small barrier disappears and therefore, the classical motion of the mass fragmentation rapidly increases up to η-values where superheavy nuclei are formed.

In Fig. 25 the classical equations are solved with friction in the adiabatic potential (f = 0). The friction force causes a slowing down of the relative motion. This can be recognized by comparing the results of Figs. 24 and 25. For the same incident energy the reaction time is diminished, and consequently a smaller mass transfer $\eta(T)$ results. If temperature effects are not included in the fragmentation potential (f = 0), the effect of friction is approximately compensated by a higher bombarding energy.

d.) Quantum mechanical treatment of η-motion: The η-motion in Eq.(28) is quantized according to the Pauli prescription. Then the wave function for the mass fragmentation is the solution of the time-dependent Schrödinger equation in which the relative coordinate $R(t)$ and its conjugate momentum $p_R(t)$, obtained from the classical calculation, are inserted.

$$H(\eta, R(t), p_R(t), t)\ \psi(\eta,t) = i\hbar \frac{\partial}{\partial t}\ \psi(\eta,t) \qquad (29)$$

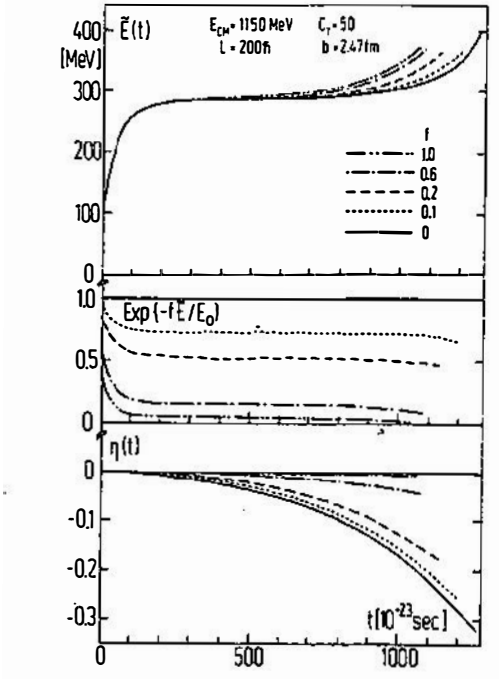

Fig. 27. The excitation energy $\tilde{E}$, the temperature-dependent factor of the shell correction energy and the classical fragmentation for various sharing ratios f in the ^{238}U-^{238}U collision.

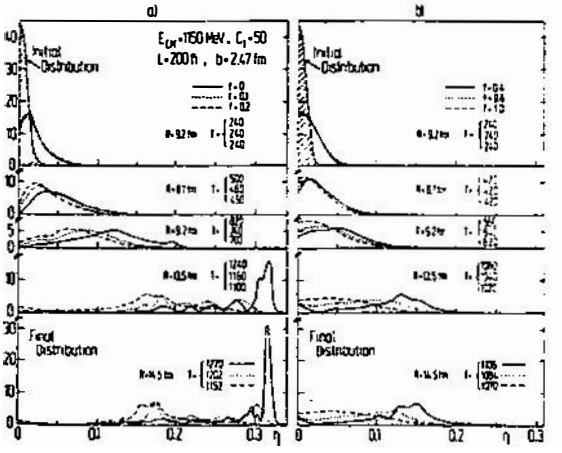

Fig. 28. The time evolution of the mass distribution for various values of f. The times are given in units of 10^{-23} sec.

Eq. (29) is numerically solved with the initial condition for $R(t=0)=R_c$:

$$\psi(\eta, t=0) \sim \exp\left[-\frac{1}{2}\left(\frac{\eta-\eta_i}{\Gamma}\right)^2\right] \qquad (30)$$

The coordinate η_i of the initial mass fragmentation characterizes projectile and target, and the width Γ the few nucleon transfer, which takes place before the critical distance R_c is reached. The critical distance R_c = 14.5 fm is assumed to be equal to the touching distance of the two nuclei. The width is chosen as Γ = 0.0126 which corresponds to a spread in the mass number of ΔA = 3.

Fig. 26 shows the time evolution of the mass distribution for the case of the adiabatic potential (f = 0) and without friction. The mass transfer is sensitively influenced by the initial choice η_i of the target and projectile combination. By comparison of Figs. 26a and b it can be seen, that for an incident energy of E_{CM} = 820 MeV the small peak at η = 0.02 plays a decisive role at the first stage of the fragmentation. If the incident fragmentation lies in the minimum of the potential at η_i = 0.118 where one of the nuclei is a Pb-nucleus, the center of the mass distribution stays around the minimum during the whole collision as shown in Fig. 26c.

In Fig. 27 we show the energy transferred from the radial motion to the other degrees of freedom for various choices of the sharing parameter f. The thermal excitation energy E_0 above which the shell effects vanish is chosen as E_0 = 95 MeV. One notes that the internal excitation energy $\tilde{E}(t)$ increases rapidly in the first stage of the reaction and keeps a nearly constant value $\bar{E}$ in the interaction region. Fig. 28 presents the time evolution of the quantum mechanical fragmentation distribution in the ^{238}U - ^{238}U collision. The final fragmentation depends strongly on the energy ratio $f\bar{E}/E_0$. We find that for an appreciable mass transfer the energy $E_\theta = f\bar{E}$, transferred into the thermal excitation, has to be less than $E_0 \approx$ 100 MeV since above this energy the shell effects in the fragmentation potential become smoothed out.

The curves in Fig. 28 for f = 1 resemble the results of the diffusion theories in which the Fokker-Planck equation is solved[32]. The diffusion theories assume a completely statistical standpoint for solving the time-dependence of the mass transfer. In contrast, our theory treats the mass transfer as a coherent collective motion, describable by quantum mechanics. When the friction in the mass transfer, which is not yet included in the theory, becomes important, the time-dependent Schrödinger equation (29) has to be replaced

by a non-linear form as suggested in Ref. 33.

e.) Production of superheavy elements: The calculated probability for producing superheavy elements ($\eta > 0.20$, $A_1 > 286$) in $^{238}U - ^{238}U$ collisions depends sensitively on the remaining shell structures in the potential as demonstrated in Fig. 28. The crucial question, namely, to what extent the shell structures are preserved during the reaction, is not yet solved. The solution depends on how fast the excitation energy is transferred into the thermal excitation of the compound system. Possibly a time-delay (retardation) between the loss of energy from the relative motion and its final appearance as temperature has to be taken into account. Such a time-delay would hinder the destruction of the shell structures.

As shown in Figs. 24 and 25 the reaction time grows with increasing bombarding energy. Increasing reaction times lead to a larger mass transfer which can be recognized in the time-evolution of the mass distribution in Fig.28. The effect is more or less independent of the sharing parameter f. Therefore, we conclude that the bombarding energy in heavy ion reactions has to be increased to obtain an appreciable mass transfer. At higher bombarding energies the U-nuclei overlap more. At larger overlaps, i.e. at smaller relative distances R, the fragmentation potential becomes flatter in η since the compound nucleus has been formed and the neck has vanished (see Fig. 22). In that case the wave function for the fragmentation can extend to the region of $\eta > 0.2$ without being hindered by a potential barrier provided that the reaction time is sufficiently long. But as discussed above, the condition of a sufficiently long reaction time is fulfilled at higher bombarding energies, Therefore, all the arguments indicate that a larger mass transfer can only be expected at higher bombarding energies. The present data[34] for U-U scattering obtained at GSI at energies of about 7 MeV/nucleon show no prominent mass transfer to masses with $A > 260$.

5.2. Quasi-Fission Reactions[35]

In the following we discuss the two step process of fission after a few nucleon transfer in the reaction of 605 MeV ^{84}Kr ions with ^{238}U. For this reaction the yield of 156 nuclides are measured radiochemically[36]. The analysis of the mass-yields, shown in Fig. 29, gives rise to five components:

1.) transfer products centered on the target and projectile masses("rabbit ears"), quasi-Kr products at $A \approx 85$,
2.) products centered slightly below $A = 119$ from the symmetric fission of the quasi-U component,

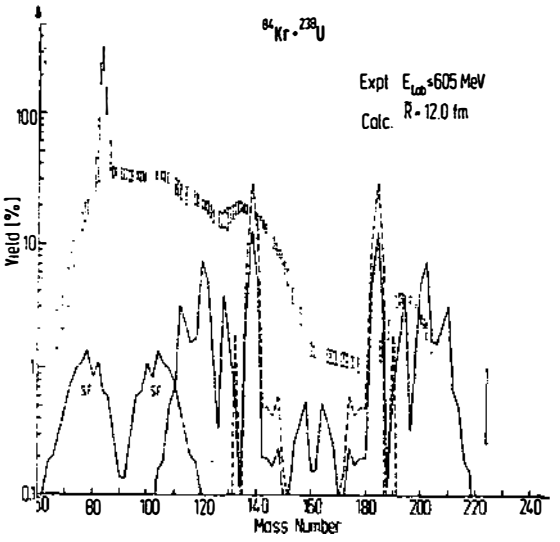

Fig. 29. The experimental[36] and calculated[35] mass yields $^{84}K + ^{238}U$.

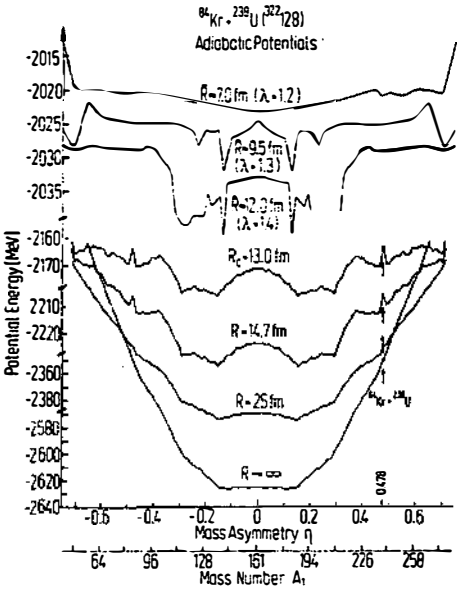

Fig. 30. Potential energy as function of η and R for the system A = 322.

3.) the heavy-mass branch at A ≈ 140 of the low energy fission products of Z ≈ 92 nuclides,
4.) products from complete fusion-fission, the broad continuous distribution at A ≈ 160 - 180
5.) an excess yield at A = 195 which is usually called "gold finger".

These components have been explained by Gupta[35] in the framework of the fragmentation theory.

The experimentally observed characteristic kinetic energy of products suggests that the initial kinetic energy is almost completely damped during the collision. Therefore, a composite, very deformed system with A = 322 and Z = 128 is formed which fissions as a normal nucleus. This allows us to calculate the mass and charge yield distributions for $^{322}128$ by exactly the same method as we have used it for fissioning nuclei in Sect. 3.1.

Fig. 30 shows the calculated potential $V(R,\eta)$ for the compound nucleus $^{322}128$. The initial system $^{84}Kr + ^{238}U$ lies at $\eta = 0.478$. Since the initial system approaches outside the potential minima, we expect that mass and charge transfers occur already near the critical radius R_c. The transfer products are centered close to the projectile and target masses. Using the potential shown in Fig. 30, Gupta has calculated the mass-yields for the fission of $^{322}128$ at $\bar{R}$ = 12 fm. The yields are drawn in Fig. 29 for the fission of the ground state (dashed lines) and of a state with 100 MeV excitation (full lines). In agreement with the experimental data, the calculated mass yield distribution does not show any maximum at the half-mass A = 161 of the composite system. The heavy-mass component appearing in the calculation around A = 180 - 190 can fission sequentially. As an illustration of this process, the sequential fission of the component A ≈ 184 (shown shaded in Fig. 29) has been calculated. As shown in Fig. 29 by the curves marked SF, the products are centered around A ≈ 80 and 104. The products lie in the same mass region as the quasi-Kr products and the light-mass branch of the low energy fission of Z = 92 nuclides.

In conclusion the fragmentation theory gives at least a qualitative description of the mass-yield distributions in the quasi-fission reaction of $^{84}Kr + ^{238}U$. Some of the experimental components appear as primary fission products in the calculation. A more quantitative comparison between theory and experiment may not be expected at this stage, since the experimentally observed yields represent only a fraction of the total mass yields[36].

6. Conclusions

In this article we have reviewed the fragmentation theory which treats the whole set of two-fragment channels of a nuclear system on a common basis. The principle idea is to describe the mass and charge fragmentation by dynamical collective coordinates η and η_Z which are continuous in the reaction zone and discrete for separated nuclei. The method has the advantage that all elements of the model Hamiltonian, such as potentials and masses can be consistently calculated. The application of the theory is very wide: Mass- and charge-yield distributions are shown to be in quantitative agreement with experiment. For the production of new elements the theory predicts an optimum choice of the target and projectile nuclei. The theory of the mass transfer in heavy ion scattering is developed as far as experimental data can be compared with calculations.

Future prospects and extensions of the fragmentation theory are the following: In the calculations of the potentials and masses we have to include the effects of nuclear temperature and nuclear rotation. The ATCSM needs asymptotic corrections in order that the Fermi-levels of the separated fragments lie at the exact relative positions[37]. In the scattering calculations also the neck-degree of freedom and the deformations have to be treated as dynamical degrees of freedom. Only the dynamical treatment of the shape parameters leads to a consistent method to distinguish between the scattering and fission channels[38]. The validity of the quantum-mechanical treatment of the fragmentation coordinate has to be investigated for the case that the nuclear compound system has been thermalized.

A generalization of the fragmentation theory to three- and more-fragment channels has recently been carried out by H.J. Fink[39]. Fink has introduced collective fragmentation coordinates for the three-body channels and solved the principal questions of their dynamics. The masses and potentials for the three-body channels have to be calculated with the general asymmetric three-center shell model. The development of these generalized shell models is in progress[40].

References

1. W. Greiner, Molecules in Heavy Ion Collisions, Proceedings of the Int. Conf. on Resonances in HI Reactions, Hvar 1977
2. H.J. Lustig et al., Proceedings of the Int. Conf. on Resonances in HI Reactions, Hvar 1977
3. H.J. Fink, W. Greiner et al., Proceedings of the Int. Conf. on Reactions between Complex Nuclei, Nashville 1974, North Holland Publ. Comp., Amsterdam, p.21; R.K. Gupta, Particles and Nuclei 8 (1977) No. 4
4. P. Lichtner, D. Drechsel, J. Maruhn and W. Greiner, Phys. Lett 45 B (1973) 175; J. Maruhn and W. Greiner, Phys.Rev.Lett. 32 (1974) 548
5. R.K. Gupta, W. Scheid and W. Greiner, Phys. Rev. Lett. 35 (1975) 353
6. H.J. Fink, J. Maruhn, W. Scheid and W. Greiner, Z. Phys. 268 (1974) 321
7. J.M Eisenberg and W. Greiner, Nuclear Theory, Vol. 1 (North-Holland Publ. Comp., Amsterdam, 197o)
8. H.J. Fink, W. Scheid and W. Greiner, Nucl. Phys. A 188 (1972) 259 and Journ. of Phys. G1 (1975) 685
9. J. Maruhn and W. Greiner, Z. Phys. 251 (1972) 431
1o. M.G. Mustafa, U. Mosel and H.W. Schmitt, Phys. Rev. Lett. 28 (1972) 1536; Phys. Rev. C7 (1973) 1519
11. V.M. Strutinsky, Nucl. Phys. A95 (1967) 42o; Nucl. Phys. A122 (1968) 1; M. Brack et al., Rev. Mod. Phys. 44 (1972) 32o
12. T. Morović and W. Greiner, Z. Naturf. 31a (1976) 327
13. S. Liran, H.J. Scheefer, W. Scheid and W. Greiner, Nucl. Phys. A248 (1975) 191
14. E.F. Chaffin and F. Dickmann, Phys. Rev. Lett. 37 (1976) 1738
15. J.A. Maruhn and W. Greiner, Phys. Rev. C13 (1976) 24o4
16. W.D. Myers and W.J. Swiatecki, Nucl. Phys. 81 (1966) 1 and Ark. Fys. 36 (1967) 343
17. H. Farrar, H.R. Fickel and R.H. Tomlinson, Can. J. Phys. 4o (1962) 1o17; Nucl. Phys. 34 (1962) 367
18. R.C. Jensen and A.W. Fairhall, Phys. Rev. 1o9 (1958) 942
19. W. John, E.K. Hulet, R.W. Lougheed and J.J. Wesolowski, Phys. Rev. Lett. 27 (1971) 45
2o. A.C. Wahl, R.C. Ferguson, D.R. Nethaway, D.E. Troutner and K. Wolfsberg, Phys. Rev. 126 (1962) 1112
21. G. Siegert et al., Phys. Rev. Lett. 34 (1975) 1o34
H.G. Clerc et al., Nucl. Phys. A247 (1975) 74 and Z. Phys. A274 (1975) 2o3
22. A. Ghiorso et al., Phys. Rev. Lett. 33 (1974) 149o and references therein
23. G.N. Flerov et al., JINR Preprint D7-9555 (1976) and references therein
24. A. Sandulescu, R.K. Gupta, W. Scheid and W. Greiner, Phys. Lett. 6oB (1976) 225

25. P.A. Seeger, CERN report No. 70-30, Vol 1., p. 217, Geneva 1970

26. R.K. Gupta et al., Further possibilities with Pb-targets for synthesizing super-heavy elements, Z. Phys. A 283 (1977) 217; Synthesis of Fermium and Transfermium-elements using ^{48}Ca-beams, preprint, Frankfurt 1977

27. R.K. Gupta, A. Sandulescu and W. Greiner, Phys. Lett. 67B (1977) 257

28. S. Yamaji, W. Scheid, H.J. Fink and W. Greiner, Z. Phys. A 278 (1976) 69; J. Phys. G2 (1976) L 189; J.Phys. G 3 (1977) 1283

29. O. Zohni, J. Maruhn, W. Scheid and W. Greiner, Z. Phys. A275 (1975) 234 and O. Zohni, Symposium on Macroscopic Features of Heavy Ion Collisions, Argonne, p. 867 (1976) and Nukleonika 21 (1976) 801

30. A.S. Jensen and J. Damgaard, Nucl. Phys. A203 (1973) 578

31. J.P. Bondorf et al., Phys. Reports 15 (2) (1974) 83

32. W. Nörenberg, Z. Phys. A274 (1975) 241 and A276 (1976) 84;
H. Hofmann and C. Ngô, Phys. Lett. 65B (1976) 97,
H. Weidenmüller, Proceedings of the Meeting on HI-Collisions, Fall Creek Falls State Park, USA 1977

33. K. Yasue, Phys. Lett. 64B (1976) 239 and J.Stat. Phys. 16 (1977) 113 and contributed paper to the Meeting on Heavy-Ion Collisions, Fall Creek Falls State Park, USA 1977

34. Jahresbericht 1976 der Gesellschaft für Schwerionenforschung, GSI-J-1-77, J.V. Kratz et al., p. 60, H. Freiesleben et al., p. 61, R. Bock et al., p. 62

35. R.K. Gupta, Z. Phys. A281 (1977) 159

36. J.V. Kratz, A.E. Norris, G.T. Seaborg, Phys. Rev. Lett. 33 (1974) 502

37. H. Gick, D. Glas and U. Mosel, Z. Phys. A 282 (1977) 417

38. A. Sandulescu and W. Greiner, University Frankfurt, 1977, preprint

39. H.J. Fink, Habilitation Thesis, University Frankfurt, 1977,

40. P. Bergmann, H.J. Scheefer, Z. Naturf. 29a (1974) 1003;
H. Diehl, W. Greiner, Nucl. Phys. A229 (1974) 29;
J. Hahn, H.J. Lustig and W. Greiner, Z. Naturforsch. 32a (1977) 215

Discussion

N. Cindro: You have shown the mass dependence of the fusion cross section for two heavy ions. Have you any results on the energy dependence?

W. Scheid: Up to now we have calculated mass yields for selected energies and impact parameters. In next future we will calculate differential cross sections as function of energy.

M.S. Weiss: While, in this theory, mass asymmetry is enhanced by high energy, will this extra energy not lead to such fast fragmentation of the heavy fragment that vitiates the super-heavy production?

W. Scheid: That is correct. Our calculations are restricted to two-body break-up channels. The fission of the heavier fragment leads to three clusters in the exit channels. This reaction can be approximately treated in the following manner: In the first step one calculates the primary distribution assuming two-body break-up channels only. In the next step the fission of the heavier fragment is taken into account according to the methods outlined in this talk. When the fission of the heavier fragment occurs already during the interaction of the two-heavy ions, the two- and three-body channels have to be treated upon the same footing (see Refs. 39 and 40).

R.W. Hasse: In deep-inelastic heavy-ion reactions with very asymmetric systems the charge-asymmetry degree of freedom equilibrates much faster than the mass asymmetry degree of freedom. The former one, hence, cannot be described by use of adiabatic cranking masses, whereas the latter probably can. Both, however, are connected by $A = N + Z$. Are you therefore shure that your cranking mass $B_{\eta\eta}$ is adequate in your dynamical model?

W. Scheid: The calculation of the masses according to the method of Inglis is based on the assumption that the collective motion is adiabaticly slow. The considered collective motions may not be adiabaticly slow. Only for reasons of simplicity we have used the cranking masses. More theoretical work is needed in order to solve the problem of collective masses in non-adiabatic motions (see Refs. 13 and 14).